1

Surfaces in Nature

Mehmet Gürsoy and Mustafa Karaman

"Natura nihil frustra facit" (Nature does nothing in vain).
<div align="right">Aristotle (384–322 BC)</div>

1.1 Introduction

Human beings have used nature in order to meet their needs. Early inhabitants took advantage of natural resources and materials just for their fundamental needs such as food, shelter, and clothing. Over the past several centuries, science and technology have developed exponentially in the world. Conventional materials and methods such as self-cleaning surfaces, new generation optical devices, biomaterials, and so on are not enough to meet the requirements of high-technology applications.

Thanks to improvements in surface analysis techniques, scientists can look deep into nature. In this way, the relationships between the structure and functions of living organisms can be investigated.

Since the beginning of life, all kinds of living organisms from one-celled creatures to plants and animals have adapted to their environments for survival. By extensive trial and error processes, nature itself has created a great number of outstanding living creatures with tested and proven sustainable biological functions. As a result of the long adaptation process (spanning millions of years), organisms have developed impressive features that have equipped them better to compete for limited resources, defend themselves against their predators, and live longer. Therefore, it can be easily said that nature is the best materials scientist ever. Because of this, copying or mimicking of biological systems is an effective way to produce desired high-technology materials. This approach is called as *biomimicry*.

The word biomimicry is a combination of two Ancient Greek words, "bios" meaning "life," and "mimesis" meaning "to imitate." Biomimicry can be defined as that branch of science that seeks to imitate processes or structures existing in nature. The main philosophy behind biomimicry is "If Nature can do it, so can we." With this approach, nature is used as a guide to tackle problems using biomimetic materials and processes.

Biomimetic innovation is based on the observation and mimicking of nature. Indeed, observation and learning from nature began in the initial days of mankind. That is why, biomimicry has been accepted as an ancient discipline. Throughout history, nature has inspired us to invent many tools.

During the Renaissance Period, numerous impressive bio-inspired designs were produced by Leonardo Da Vinci. For instance, he designed a flying machine by investigating bird anatomy. His words on nature show why he applied bio-inspired idea on his designs: "Although human genius through various inventions, makes instruments corresponding the same ends, it will never discover an invention more beautiful, nor more ready, nor more economical than does nature, because in her inventions nothing is lacking and nothing is superfluous [1]."

In 1969, the term *biomimetics* was first used by bioengineer Otto Herbert Schmitt in his paper at the Third International Biophysics Congress in Boston [2]. However, biomimicry was popularized by Janine Benyus in her book Biomimicry: Innovation Inspired by Nature (1997) [3]. Subsequently, biomimetic approaches have become more and more popular and important during the past decades in almost all research fields.

There have been a lot of studies in materials science, based on mimicking natural materials. In this chapter, examples of biomimetic materials, especially the related surfaces, are given.

1.2 Inspiring Natural Surface Structures

1.2.1 Self-Cleaning Surfaces

Self-cleaning surfaces are in great demand for fundamental research and various industrial applications. These types of surfaces must have two important criteria: very high contact angle and low contact angle hysteresis.

Contact angle can be defined as a measure of the wettability of a solid surface by a liquid drop (Figure 1.1a). Theoretically, the contact angle values must be between 0° and 180°. If the contact angle is less than 90°, these surfaces are classed as hydrophilic. If the wetting angle is higher than 90°, these kind of surfaces can be accepted as water repellent. When a contact angle approaches 180°, the surface is considered superhydrophobic. Adhesion of droplets on the surface can be determined by dynamic contact angle measurements. Dynamic contact angle is referred as *advancing contact angle* (the maximum value of the contact angle) and *receding contact angle* (the minimum value of the contact angle). Contact angle hysteresis is the difference between them. There is a strong relation between sliding angle and contact angle hysteresis. Sliding angle is the required minimum angle to move the droplet on surfaces (Figure 1.1b). As the contact angle hysteresis decreases the drops can easily roll off from the surfaces.

In nature, self-cleaning properties have been observed in various plant leaves. On a rainy day, the raindrops do not spread on the plant leaf and these drops completely roll off the leaf. And thus, undesirable particles on the leaves are easily removed by rolling water drops. It is also known that pathogenic microorganisms
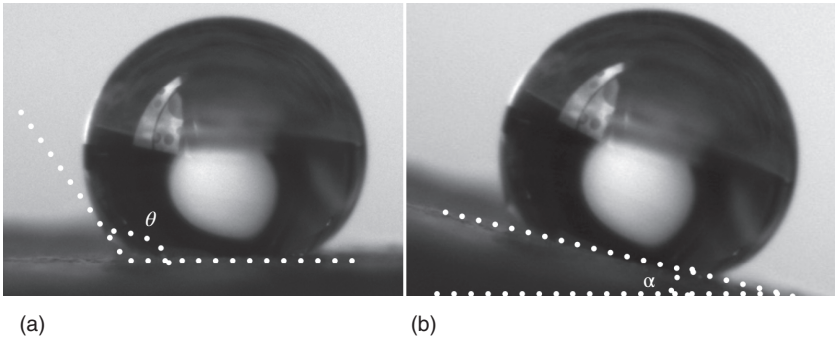
(a)   (b)

Figure 1.1 (a) θ is the water contact angle and (b) α is defined as the inclination angle at which a water drop rolls off the surface.

cannot germinate and infect leaves without water. For this reason, self-cleaning helps prevent the occurrence of plant diseases [4].

Among the plants that are self-cleaning, lotus is one of the most popular examples due to its very high contact angle and very low hysteresis. These values are 164° and 3°, respectively [5]. That is why, the term *Lotus Effect* is also used in place of "Self-Cleaning Effect" in the literature [6]. The lotus grows in an aquatic environment such as lakes, and shallow and muddy water. It always achieves to remain clean even in dirty waters [7, 8]. For this reason, the lotus is considered as a symbol of purity.

The plants are covered by a cuticular surface except for their roots. The cuticle layer is a natural composite that is the interface between plants and their environment [9]. This composite consists mostly of two parts, soluble lipids and bio-polyesters [10, 11]. Because of the chemical structures of these components, the cuticle layers usually exhibit hydrophobic properties. Lotus leaf surface is also covered by low surface energy cuticular surface, which contains mainly —CH_2— groups [12]. The relation between the contact angle and surface energy was formulated in Young's Eq. (1.1) describing wetting phenomena in terms of thermodynamic equilibrium [13] (Figure 1.2).

$$\cos \theta = \frac{\gamma_{SV} - \gamma_{SL}}{\gamma_{LV}} \tag{1.1}$$

where θ is the contact angle of the liquid, γ_{SL} is the interfacial surface tensions between the solid and the liquid, γ_{SV} and γ_{LV} are the solid and liquid surface free energy, respectively. According to Eq. (1.1), decreasing γ_{SV} should increase the contact angle value.

However, it is well known that the lower surface energy of —CH_3 groups or fluorocarbons do not exist in any biological systems [12]. So, the contact angle of

Figure 1.2 The schematic representation of a liquid drop with the contact angle and tension vectors.
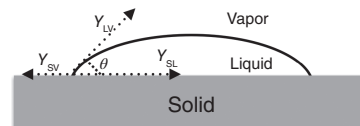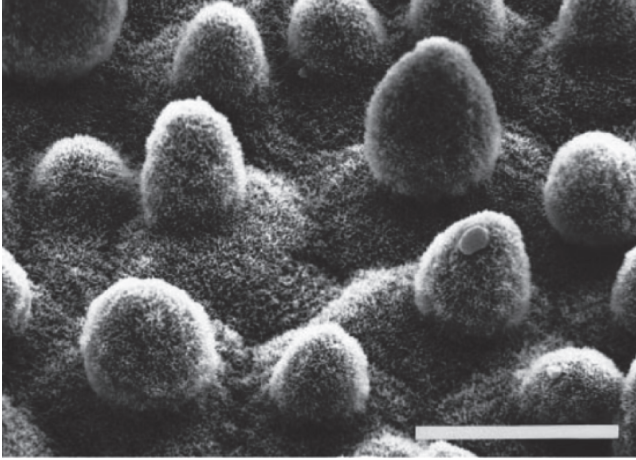
Figure 1.3 The SEM image of adaxial lotus leaf surface, scale bar = 20 μm. (Barthlott 1997 [9]. Reproduced with permission of Springer.)

a planar cuticular surface can be a maximum of about 110° [14]. Thus, in nature only having low surface energy surface is not enough to be superhydrophobic. By means of scanning electron microscope (SEM), micrometer scale bumps and nanometer scale wax crystals were observed on the lotus leaf surface [9]. The SEM image of adaxial lotus leaf surface structure is given in Figure 1.3.

The effect of surface roughness on the wettability can be explained with the help of the Wenzel model [15, 16]. The Wenzel model describes the following Eq. (1.2).

$$\cos \theta = R_f \cos \theta_0 \tag{1.2}$$

In which, θ is the contact angle of a rough surface, θ_0 is the contact angle of a smooth surface, and R_f is the surface roughness factor. The roughness factor is defined as the ratio of the actual surface area to the geometric surface area. If the surface is flat, $R_f = 1$; however, this value must be higher than 1 for rough surfaces. For a hydrophilic surface, θ_0 must be lower than 90°, roughness decreases the contact angle. On the other hand, for hydrophobic surfaces, as in lotus leaf, θ_0 is greater than 90°. Therefore, according to Wenzel equation, it is expected that increasing the surface roughness increases hydrophilicity [17].

In brief, water repellent surfaces can be produced in two different ways: changing the surface morphology and decreasing the surface free energy. In the former method, the underlying principle is to create micro/nanoscale rough structures on the surfaces. In the latter method, the surfaces are usually coated with hydrophobic functional groups. Only having low surface energy or only having rough surfaces may not be sufficient to be superhydrophobic. Thus, the production of superhydrophobic surfaces mostly requires the combination of two methods.

The extraordinary surface morphology of lotus leaf minimizes the contact area between its surface and water drops. The hierarchical micro/nanostructures

provide that air is trapped underneath the water drop. That is why, very high contact angle values are observed on the lotus leaf. The unique structure of the lotus leaf can be directly imitated in order to produce self-cleaning materials.

Roughening fluorinated polymers and silicones directly leads to superhydrophobic surfaces, because of the inherent hydrophobic nature of these kinds of polymers. For example, Barshilia and Gupta [18] treated polytetrafluoroethylene (PTFE/Teflon) surfaces with argon and oxygen plasma to obtain a superhydrophobic surface. The highest average water contact angle and the maximum surface roughness were found for 4 h plasma treatment. During plasma treatment, inspite of changing the surface morphology, functional groups were preserved. The contact angle value increased from 102° to 158°. After 10 months, the contact angle was again measured from the modified surface and almost the same values were found. According to the results, the superhydrophobicity of obtained surface remains unchanged even after a long time. Similarly, Jin *et al.* [19] created a polydimethylsiloxane (PDMS) surface containing micro-, submicro-, and nanostructures using a one-step laser etching method. Etched PDMS surface with these special structures showed high water contact angle (162°) and low sliding angle (< 5°).

Coating rough or hierarchical surfaces with low surface energy materials is also a common method to produce self-cleaning materials. Ma *et al.* [20], produced superhydrophobic fabrics by a two-step process. In the first step, poly(caprolactone) (PCL) fibers were generated by the electrospinnig method. And then, the fiber mat surfaces were coated with perfluoroalkyl ethyl methacrylate (PPFEMA) by Initiated Chemical Vapor Deposition (iCVD). These PFEMA-coated electrospun fibers exhibited very good self-cleaning properties with contact angle of 175° and sliding angle of lower than 2.5°. These results are attributed to the combination of the inherent roughness of the electrospun mats and the low surface energy of the PPFEMA coating. Liu *et al.* [21] fabricated micro-nanoscale binary structured composite particles of silica/fluoropolymer using an emulsion-mediated sol–gel method to mimic the surface microstructures on the lotus surface. With this method, super hydrophobic surfaces with water contact angle larger than 150° were obtained. Grewal *et al.* [22] investigated the effect of different micro- and nanopatterned surfaces on their wettability and tribological surfaces. The hierarchical patterns were designed, imitating the topography of the adaxial surface of lotus leaf. The advancing and receding contact angle of PTFE-coated hierarchical structure surface was found to be similar to those of the lotus leaf.

The casting method (soft molding) is another simple and effective way to replicate leaf surface structures. Sun *et al.* [23] successfully applied this method for lotus leaf at the first time. They cast PDMS on the lotus leaf, and then the PDMS layer was peeled off. After that, this negative PDMS layer was used to make a positive PDMS layer. According to SEM results, the positive replica and the original lotus leaf showed the same surface structures. The positive template also exhibited similar superhydrophobic properties as the fresh lotus leaf. The contact angle of the positive replica was found as 160° and the water droplets could easily roll off this surface.
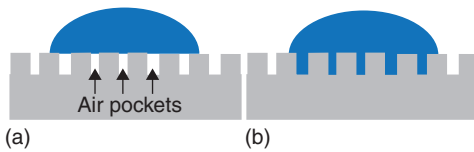
Figure 1.4 (a) Cassie model wetting regime and (b) Cassie impregnating wetting regime.

1.2.2 Adhesive Hydrophobic Surfaces

Similarly to lotus leaves, the hierarchical nano- and microstructures on the red rose petal surface provide a high contact angle. However, differently from lotus leaves, water droplets do not slide off the surface of a red rose petal.

Basically, two main hypotheses are used to explain superhydrophobicity on rough surfaces: Wenzel and Cassie wetting regimes. The former regime has been already mentioned in the beginning of this chapter. The Cassie model was developed after the Wenzel's state. According to the Cassie model [24], air is trapped in micro- and nanostructures underneath the water droplets, as seen in Figure 1.4. Because of these air pockets, the liquid cannot wet the surface. It is thus expected that water drops easily roll off this kind of surface, just as in the lotus leaf. The wetting mechanism of lotus leaf is an excellent example for Cassie wetting regime. On the other hand, spherical water droplets usually stick on the red rose petal surfaces. This different behavior can be attributed to difference in the surface topography between the red rose petal and lotus leaf. It is observed that the sizes of the structures on the red rose petal are larger than those of lotus leaves [25]. While water drops cannot enter into the grooves of the lotus surface, they can enter into the grooves of the red rose petal surface.

This phenomenon is known as the *Cassie impregnating wetting regime* as seen in Figure 1.4 [26]. Due to the high adhesion between the water drops and petal surface, the petal surface exhibits a high contact angle. Therefore, water droplets do not fall off even if the petal surface is tilted to 180°. The unique wettability behavior of red rose petal surface was defined as the "petal effect" by Feng *et al.* [27] for the first time in the literature. Recently, there has been a great deal of interest in fabrication of artificial "petal effect" coating and surfaces that mimic the original red rose petal.

Karaman *et al.* produced a thin "petal effect" polymer sheet using a combination of casting and iCVD methods [28]. Firstly, they poured poly vinyl alcohol (PVA) solution on the surface of a fresh red rose petal. The obtained PVA negative mold was placed in an iCVD reactor, then coated by poly(glycidyl methacrylate) (PGMA) and poly(1*H*,1*H*,2*H*,2*H*-perfluorodecyl acrylate) (PPFDA). This schematic duplication process of the red rose petal surface is presented in Figure 1.5. The contact angle of the positive replica was found as $152 \pm 3°$ and the water did not roll off even when the biomimetic polymer sheet was turned upside down.

Fluorinated polyimide was synthesized by the electrospinning method by Guangming *et al.* [29]. The surface of nanofibers consisted of dented nano- and/or micro bowl-like structures. The air is trapped in bowl-like particles below the water droplets; this situation provides a very high contact angle. Moreover, when the droplet is lifted, the air pocket expands, which creates a negative pressure, and thus the adhesion between water droplet and surface is increased.
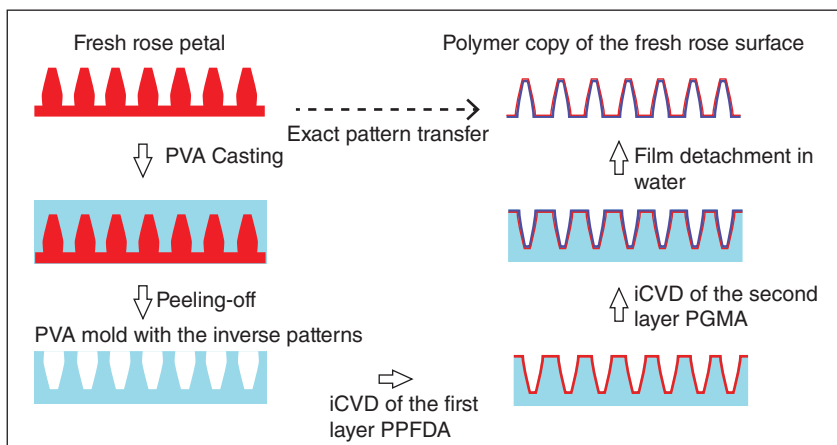
Figure 1.5 The schematic duplication process of the red rose petal surface. (Karaman 2012 [28]. Reproduced with permission of Elsevier.)

The maximum adhesion force of the petal effect surface was measured as 127 μN and the contact angle was found as 153°.

Recently, the tunable adhesive superhydrophobic surfaces have been produced by controlling the reaction parameters, such as reaction time, particle sizes, surface roughness, and so on. In other words, superhydrophobic surfaces having tunable water adhesion capability allow choosing wetting behaviors, "lotus effect" or "petal effect." For instance, Liu *et al.* [30] developed a one-step electrodeposition process in that, superhydrophobic surfaces with controlled adhesion can be easily produced by just changing the reaction time. When the reaction time is 10 min, a petal effect surface was obtained and the maximum contact angel was found as 155.1°. When the reaction time increased further up to 30 min, a self-cleaning surface was obtained. Its static contact angle and contact angel hysteresis were found to be 161.7° and 3°, respectively.

Another fabrication of superhydrophobic surfaces with tunable water droplet adhesion was carried out by Xie *et al.* [31]. They used both O_2 plasma etching and plasma deposition of thin films to create a superhydrophobic wood surface. Firstly, wood substrates were exposed to O_2 plasma, and then were coated with pentafluoroethane (PFE) films. The obtaining surfaces showed lotus effect properties with high contact angle (161.2° ± 1.5°) and low sliding angle (~15°). When wood samples were coated with diamond-like carbon (DLC) after the etching property, thees surfaces also exhibited high contact angle (153.7° ± 2.7°). However, differently from PFE-coated wood, DLC-coated samples showed a petal effect.

1.2.3 Unidirectionally Superhydrophobic Surfaces

In superhydrophobic structures that show lotus effect property, having low contact angle hysteresis is not enough for some applications, the unidirectional movement of water is also important. The water droplets move in all directions on the lotus leaf surfaces. On the other hand, the water drops on rice leaf surfaces
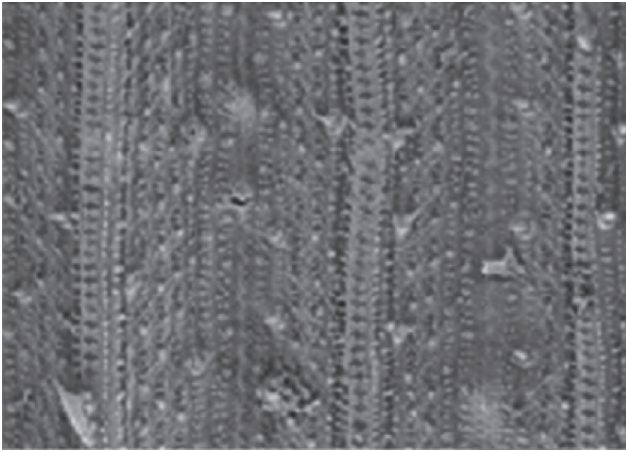
Figure 1.6 The SEM image of adaxial rice leaf surface [35]. (Yao http://link.springer.com/article/10.1007/s11434-012-5220-1. Used under CC BY 4.0 https://creativecommons.org/licenses/by/4.0/.)

roll along just the long-axis direction [32]. The difference between lotus leaf and rice leaf can be attributed to surface topography. Actually, there are similar structures on both these natural surfaces. However, while these microstructures are randomly located on a lotus leaf, they are set on a one-dimensional order (parallel to the leaf edge) on the rice leaf [33]. This observation is consistent with the difference between the parallel and perpendicular direction sliding angles on the rice leaf. These values of parallel direction and perpendicular to the leaf edge were found as $3-5°$ and $9-15°$, respectively [34]. Rice leaf surface structure is an excellent example for the fabrication of unidirectionally superhydrophobic surfaces. The hierarchical structures can be seen in Figure 1.6 [35].

Yang *et al.* used the combination of lithography- assisted electrochemical etching, anodic oxidation, and fluoridation methods to fabricate artificial rice leaf structures [36]. They achieved to fabricate a three-level microstructure (macro/micro/nano) of rice leaves on aluminum. This biomimetic structure shows superhydrophobicity and anisotropic sliding behavior.

Zhu *et al.* fabricated the large area surface with ordered binary structure arrays by mimicking the rice leaf surface structure [37]. The underlying pattern on the substrate can be easily modified by changing the polymer solution concentration, which provides the fabrication of various topographies. The obtaining surfaces demonstrate anisotropic wettability similarly to rice leaf.

In another study, Yao *et al.* developed a two-step soft transfer to produce an artificial rice leaf structure [35]. The obtained biomimetic rice surface exhibited superhydrophobicity and anisotropic sliding properties that were similar to those of natural rice. Parallel and perpendicular sliding angles were found as 25° and 40°, respectively.

Wu *et al.* used improved laser interference lithography to fabricate micropearl arrays for adjusting two-directional unidirectional wetting structures [38]. They systematically investigated the effect of laser beam intensity ratio and resin

thickness on anisotropic wetting behavior. According to appropriate parameters, micropearl arrays were designed and modifying them with fluoroalkylsilane created biomimetic surfaces exhibiting wettability properties very similar to those of rice leaf.

1.2.4 Fog Harvesting Surfaces

Access to safe and sufficient water is of vital importance to people. However, water scarcity is one of the major environmental issues, in today's world. According to World Health Organization (WHO) reports, an estimated 2.5 billion people have no access to improved sanitation and, unfortunately, each year hundreds of thousands children die from water-related diseases such as diarrhea [39–41]. Learning from living creatures that live in arid conditions is an efficient way to obtain clean water. For instance, Namib Desert beetles (*Stenocara*) overcome the lack of water by collecting moisture from air. Actually, collecting fine fog droplets is not easy in the heat and breeze of the desert. The fog collecting of mechanism of Stenocara was revealed by Parker and Lawrence. They discovered an array of hydrophilic bumps on the beetle backs, which are surrounded by hydrophobic waxy lines [42]. The fine moisture droplets collect on hydrophilic bumps and start to grow. When the collecting droplets reach sufficient weight, they detach and roll down the tilted hydrophobic beetle's back surface to the mouth. The hierarchical structures on the Namib Desert beetle's back can be seen in Figure 1.7 [42].

Zhai *et al.* successfully mimicked the back of the Stenocara beetle creating hydrophilic patterns on superhydrophobic surfaces [43]. Garrod *et al.* used a two-step plasma chemical method to produce the hydrophilic–hydrophobic pattern, which is similar to the Stenocara beetle's back [44]. Another study that is inspired by the fog harvesting surface structure of the Stenocara beetle's back was carried out by Dorrer and Rühe [45]. They fabricated various superhydrophobic surfaces patterned with smooth, circular patches of hydrophilic domains. According to the results, it was found that the pinning force for a given pump was constant and independent of the drop volume. Except for the Namib Desert beetle, some other organisms have water collection ability. Cactus is one of these organisms. It can survive in extremely arid conditions because of its efficient fog collection mechanism. A cactus consists of conical spines
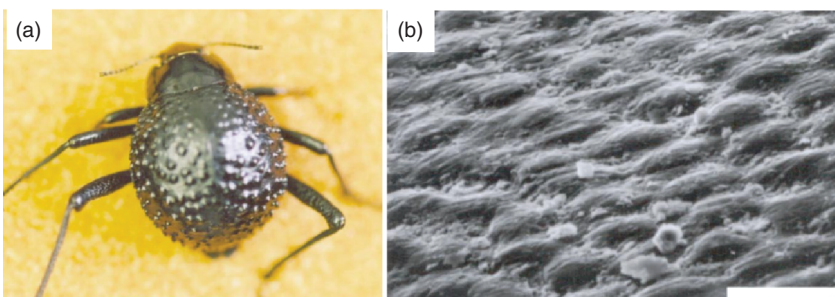

Figure 1.7 (a) The photo of an adult female *Stenocara* sp. and (b) the SEM image of the *Stenocara* sp. dorsal surface, scale bar = 10 μm. (Parker 2001 [42]. Reproduced with permission of Nature Publishing Group.)
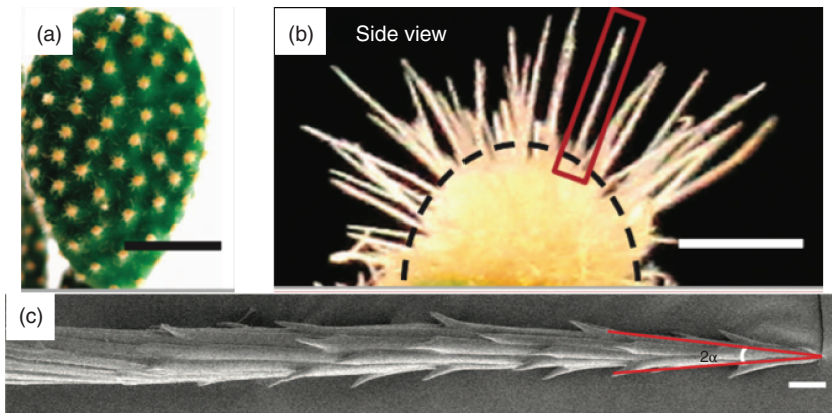
Figure 1.8 (a) The photograph of the cactus *Opuntia microdasys* scale bar = 5 cm, (b) the photography of a single cluster containing a lot of spines, scale bar = 100 mm, and (c) the SEM image of the spine, scale bar = 20 μm. (Ju 2012 [46]. Reproduced with permission of Nature Publishing Group.)

and hierarchically hydrophilic/hydrophobic structures [46]. The fog collection system of cactus is based on the Laplace pressure gradient and the wettability difference [47–49]. The hierarchical structures of the cactus' spines can be seen in Figure 1.8 [46]. Cao *et al.* produced biomimetic microtip arrays, which are similar to those of cactus, using a modified magnetic particle-assisted molding method [49]. The morphology of the tips is adjusted by changing the weight ratio of PDMS to magnetic particles. The optimal ratio of PDMS to magnetic particles was found to be 2 : 1. Andrews *et al.* reported that the *Cotula fallax* plant can also collect water from moisture due to its unique hierarchical 3D arrangement formed by its leaves and the fine hairs covering them [50].

1.2.5 Anti-reflective Surfaces

Anti-reflective coatings are used in many technological applications such as glasses computer screens, solar cells, military hardware, and so on. The purpose of using anti-reflective coating is to maximize the transmission of light through an optical surface [51].

In nature, anti-reflective structures are found in some insects. These structures can be found in their eyes, which make it possible to see objects in even low-light environments. These natural anti-reflective structures can also be found on their body surface that helps in hiding from enemies by reducing reflections [52]. For example, the eyes of the moth consist of hexagonal arrays that reduces optical losses. The dimensions of this structure are smaller than the wavelength of the light, so the reflection of light is effectively suppressed [53]. The hierarchical structure of the moth eye is shown in Figure 1.9 [54].

Moth eyes inspired anti-reflective structures that have been fabricated by various methods. One of these studies was carried out by Raut *et al.* [55]. They produced anti-reflective structures using "sacrificial layer mediated nanoimprinting." For wavelengths between 400 and 1000, while non-anti-reflective
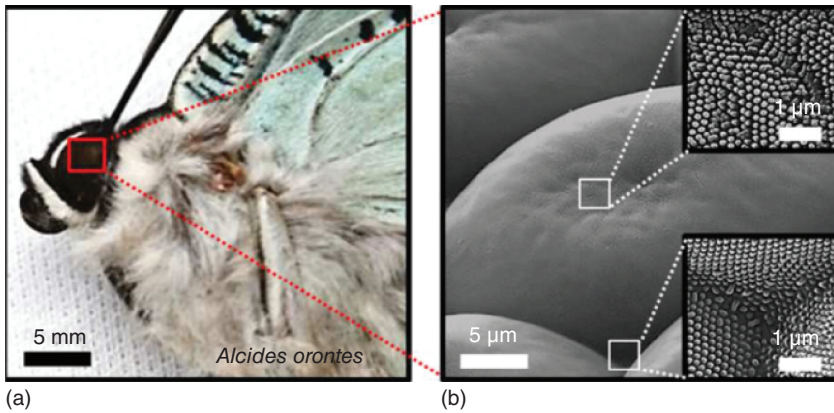
Figure 1.9 (a) The photograph of the moth *Alcides orontes* and (b) SEM images of real moth-eye structures of the moth. (Kwon 2016 [54]. Reproduced with permission of American Chemical Society.)

structures reflected 8.7% of light, the moth-inspired arrays reflected just 4.8%. The minimum reflectance was found to be 1.4% from 400 to 1000 nm in wavelength, when the arrays were designed on both sides of the substrate. Oh *et al.* also replicated the structure of moth eyes using thermal imprinting processes and plasma treatment methods [56] and with their study, the sub-wavelength structures were obtained. Except for moth eyes, other organisms also inspire researchers to design anti-reflective structures. For instance, Li *et al.* mimicked the surface of the eyes of the butterfly, *Euploea mulciber*, which consists of the hierarchical nipple array structure, in order to obtain anti-reflective structures [57]. They fabricated biomimetic amorphous carbon structure using a one-step vacuum sintering method. This structure exhibited a reflectance of 2–3% in visible light; this value for an amorphous carbon plate (without hierarchical nipple array structure) was 11% reflectance. Xu *et al.* were inspired from mosquito eye structures to produce anti-reflective structures [58]. With this aim, they used a combination of self-assembled polymer spheres and nanoimprint lithography. It was found that the topography of this biomimetic surface is similar to that of mosquito eyes. Because of the hierarchical structures, the surface reflection was considerably decreased.

1.2.6 Structural Color

Color is perhaps the most diverse property in biological creatures. The coloration in the animal kingdom provides adaptation to the surrounding environment for misleading their enemies [59]. It can also be used for sexual interactions [60]. Basically, the color source can be classified into three groups: pigments, bioluminescence, and structural colors [61, 62]. Pigmental color is known as *chemical color*, and is obtained by selective absorption of visible light by pigments [61]. Bioluminescence is produced by chemical reactions in the living organisms. Structural color is known as *physical color* that is highly related to surface structure, and is based on the nano- and microstructures on surfaces.
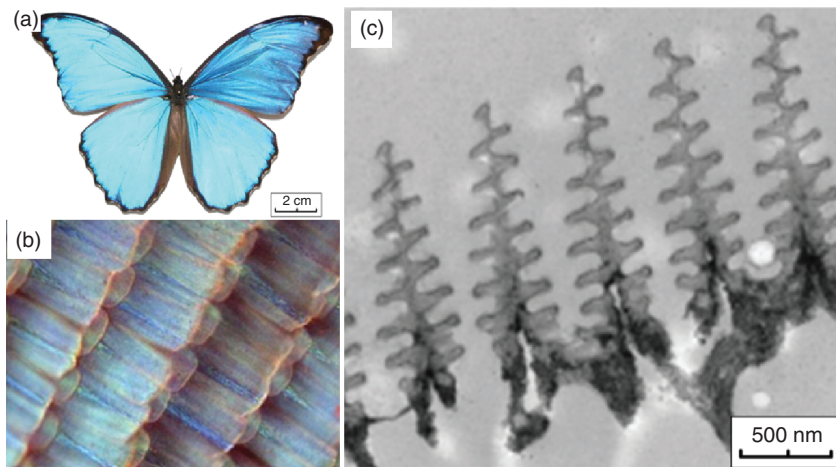
Figure 1.10 (a) The photograph of *Morpho didius* butterfly, (b) the magnified image of wing, and (c) the cross-section TEM image of wing scales. (Jiang 2014 [66]. Reproduced with permission of Elsevier.)

In contrast to chemical colors, structural colors show high resistance to discoloration because of chemical and thermal changes. According to archeological finds, structural colors in fossils are preserved as long as the structure details are maintained [63]. Moreover, when compared to pigment color, structural color is more efficient in terms of energy consumption [59]. Differently from the pigment-based color materials, physical colors can be produced without hazardous chemicals, which makes fabrication of structural colors safe and eco-friendly [64]. Due to all these advantages, the structurally based colors have drawn great interest in the past years.

In nature, there are many bright and vivid structural colors in living creatures. *Morpho* butterflies, which belong to the Nymphalidae family, are one of the excellent examples of structural color [65]. Figure 1.10 shows (a) The photograph of *Morpho didius* butterfly, (b) the magnified image of wing, and (c) the cross-section TEM image of wing scales [66].

The iridescent metallic blue color of morpho butterflies is a result of the microscopic structures on their wings, which reflect the light in order to produce this color – without pigments. The electron microscope was first used to observe the wing surface of Morpho, and ordered microstructures were found [67]. Inspiring this unique nanostructure that nature has created, biomimetic materials are produced. For example, Watanabe *et al.* used ion beam chemical vapor deposition (FIBCVD) method to mimic the structure of the Morpho wing [68]. The obtained structure morphology is almost the same as that of Morpho. Both Morpho butterfly and the replica exhibited very similar reflection intensity spectra for the various incidence angles. Another fabrication of morpho blue color was performed by Saito *et al.* [69]. They coated TiO_2/SiO_2 layers on stepped quartz using a combination of electron-beam lithography and dry etching.

Apart for insects, structural colors were also observed in some birds. Peacock is one of them, the beautiful colors of its tail feather are based

on physical color. Cong *et al.* fabricated crystal thin film composed of poly(styrene-methylmethacrylate-acrylicacid) (P(St-MMA-AA)) on an inclined silicon substrate [70]. The different colors were obtained from the different layers of stair-like thin film. With this study, the colors of the peacock's tail feathers were successfully mimicked.

1.2.7 Drag Reduction and Antifouling Surfaces

Nature has created various organisms that have special shapes and surfaces in order to reduce drag in air and water. By this means, animals can move faster by consuming low energy [71, 72]. Shark is one of this type of animals. Besides their aerodynamic shapes, they have unique skin structures. During long-term evolution, their skin structures have been optimized in order to minimize the frictional resistance between the water and their body. This makes sharks one of the fastest animals in the ocean. Shark skin is covered with tooth-like scales also called *dermal denticles*, which are aligned along the direction of water flow [73−75]. These microstructures on shark skins reduce not only water friction during swimming but also prevent bacterial growth on their bodies [76, 77]. This self-cleaning mechanism is quite different from those of the lotus and the rose petal effect. Shark skin is not superhydrophobic; in fact, it is even hydrophilic [76]. The reason for having a clean surface can be attributed to the rough shark skin structures that reduce the contact area for adhering and fouling marine organisms. In addition to surface area, the contact time is also decreased because of the accelerated flow rate on the shark's body surface [78, 79].

Inspired by the unique surface structures of shark skin, there are many studies in the literature to obtain antifouling coatings. One of these studies was carried out by Carman *et al.* [80]. They fabricated various patterns (pillars, pits, ridges, channels) on polydimethylsiloxane elastomers (PDMSe) surfaces using photolithography method. They reduced the settlement of Ulva spores by 86% when compared to smooth PDMS. Wen *et al.* used 3D printing to produce thousands of artificial shark denticles on membrane [81]. According to the results, while swimming speed is increased by 6.6%, energy cost-of-transport was reduced by 5.9%. Han *et al.* created biomimetic shark skin by direct replication of the shark skin structure [82]. The skin of *Carcharhinus brachyurus* was used as a template. This artificial sharkskin structures demonstrated a drag reduction efficiency of 8.25%. The SEM images of the natural and biomimetic shark skin structures are given in Figure 1.11a,b, respectively.

Not only marine creatures, but also birds have excellent drag reduction properties. Because of their body shape and feather structures, the birds minimize air drag and thus, they exhibit excellent flying performance. That is why researchers investigate birds in order to reduce air friction. For instance, Chen *et al.* mimicked the herringbone riblets of pigeon feathers [83]. In this study, the drag reduction efficiency of herringbone riblets was found to be 16%.

1.2.8 Adhesive Surfaces

Adhesive tapes have been widely used since their in 1845 [84]. They can be easily used without the need for any solvent or heat, these properties make them very
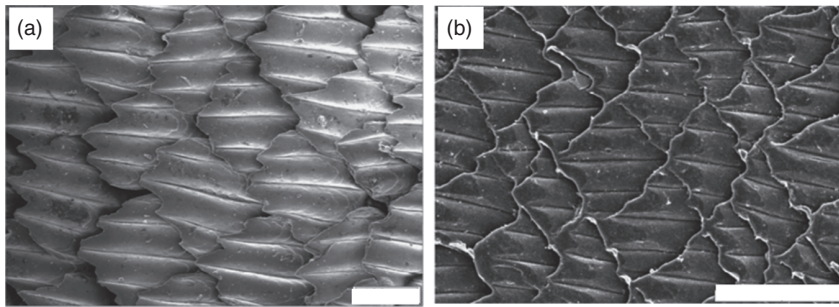
Figure 1.11 (a) The SEM image of the shark skin template and (b) the SEM image of the biomimetic shark skin. Scale bars, (a) 100 μm and (b) 200 μm . (Han 2008 [82]. Reproduced with permission of Springer.)

versatile and practical for various purposes. However, the traditional adhesive tapes cannot be used for hanging heavy objects. Moreover, they do not work under vacuum conditions [85]. Researchers seek for a solution in nature in order to produce alternative adhesive tapes without these handicaps.

The adhesive types in nature can be roughly categorized into two groups: (i) wet adhesion and (ii) dry adhesion. The former is based on secreted body fluids between the animal surface and the object [86]. This adhesion mechanism is widely observed in insects, for instance the wet adhesion was found in *Hemisphaerota cyanea* beetle [87].

In dry adhesion, mainly van der Waals bonding plays an important role and this force is generated as a consequence of the interaction between animal adhesive pads and objects [76]. The gecko lizard is a famous example of this kind of adhesion mechanism. The skin of gecko pads consists of well-aligned hairs (setae), which end in spatulae [88, 89]. The hierarchal nano- and microstructures provide enough van der Waals force to overcome gravity and, thus, geckos climb vertical surfaces and can stick to them upside down [90]. In fact, the similar hierarchal structures and micro spatulae are also observed in other animals such as insects and arachnids [91]. As can be seen in Figure 1.12, the diameters of the setae decrease with the body weight of the creature, in other words, the amount of setae per unit area increases with the weight of the animal. The gecko displays the highest density of setae, and it is also the biggest creature that generates dry adhesion [78].

Therefore, the gecko is one of the most spectacular living being for researchers to mimic its adhesive properties. One of these studies was carried out by Qu *et al.* [92]. They used a combination of PECVD and fast heating method to fabricate vertically single-walled carbon nanotubes (VA-SWNTs). It was reported that the VA-SWNTs show the highest achievable force (29.0 N cm^{-2}) among all of the synthetic and natural gecko feet. Cho *et al.* used anodic aluminum oxide (AAO) membrane with the controllable pore channels as a replication template to fabricate gecko-inspired hairy hard PDMS films with nanopillars [93]. The obtained structures showed high adhesion and superhydrophobicity. Therefore, when a water droplet is placed on this structure, it does not roll even if the biomimetic polymer sheet is turned upside down. The reason for this "petal
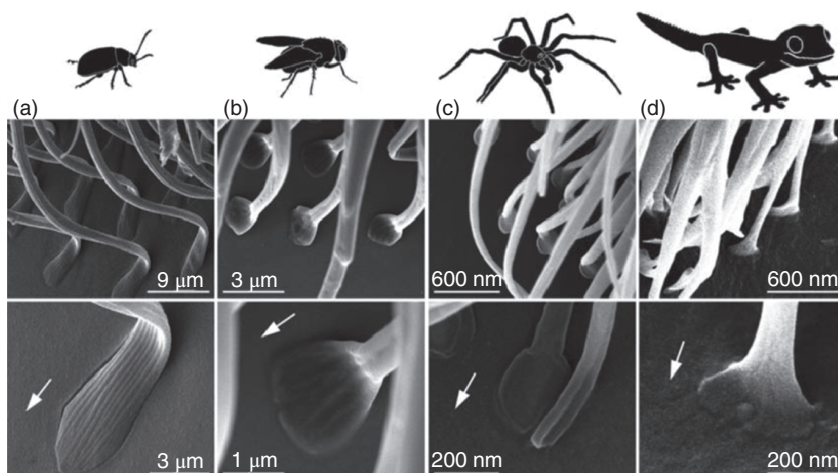
Figure 1.12 SEM images of the spatula-shaped terminal elements of various animals which have adhesive foot. (a) The beetle *Gastrophysa viridula*, (b) the fly *Calliphora vicina*, (c) spider *Cupiennius salei*, and (d) the gecko *Gecko gekko*. Arrows point in distal direction. (Varenberg 2010 [91]. Reproduced with permission of Royal Society of Chemistry.)

effect" can be attributed to van der Waals forces between the water droplets and the molded surface composed of densely packed hairy PDMS nanopillars. Davies *et al.* produced artificial PDMS-based gecko hair arrays using photolithographic and nano-molding techniques [94]. Gecko inspired wafer-scale nanofabrillar structures were produced by Kustandi *et al.* using the combination of colloidal nanolithography, deep silicon etching, and nanomolding methods [95]. Geim *et al.* produced microscale polyimide flexible plastic pillars using e-beam lithography and oxygen-plasma dry etching [96]. These gecko-inspired hierarchical structures exhibited high adhesion properties. Kim *et al.* used replica-molding and e-beam exposure methods to fabricate high aspect-ratio polyurethane acrylate nanohairs [97]. According to frictional-adhesion test results, these biomimetic structures showed good adhesion strength even after more than 100 cycles of attachment and detachment.

1.3 Conclusion

In this chapter, surface structures of various organisms have been presented, which inspire researchers to design high-technology materials. The underlying surface morphology and functions of these mechanisms have been summarized with biomimetic examples. It is obvious that the hierarchical surface nano/microstructures of both organisms and materials determine functional properties such as superhydrophobicity, anti-reflective, and so on. Some organisms have more than one property; for instance, gecko foot skin structures exhibit not only high adhesion but also superhydrophobicity. Nature has already developed a wide range of organisms and, therefore, just by copying their structures without any further tests, they can be used for the desired practical

applications. This makes the biomimicry approach a time-saving process. We believe that when considered in the greatness of nature, undiscovered functional organism surface structures must wait for mankind to mimic and use them in many fields of technology.

References

1 Thompson, B.S. (1999) Environmentally-sensitive design: Leonardo WAS right!. *Mater. Des.*, **20**(1), 23–30.

2 Schmitt, O.H. (1969) Some interesting and useful biomimetic transforms. Third International Biophysics Congress, vol. **1069**, p. 197.

3 Benyus, J.M. (1990) *Biomimicry: Iinnovation Inspired by Nature*, William Morrow and Company, New York.

4 Bhushan, B. (2012) *Biomimetics: Bioinspired Hierarchical-Structured Surfaces for Green Science and Technology*, Springer Science & Business Media, Columbus, OH.

5 Koch, K., Bhushan, B., Jung, Y.C., and Barthlott, W. (2009) Fabrication of artificial Lotus leaves and significance of hierarchical structure for superhydrophobicity and low adhesion. *Soft Matter*, **5**(7), 1386–1393.

6 Marmur, A. (2004) The lotus effect: superhydrophobicity and metastability. *Langmuir*, **20**(9), 3517–3519.

7 Latthe, S.S., Terashima, C., Nakata, K., and Fujishima, A. (2014) Superhydrophobic surfaces developed by mimicking hierarchical surface morphology of lotus leaf. *Molecules*, **19**(4), 4256–4283.

8 Shirtcliffe, J.N., McHale, G., and Newton, M.I. (2009) Learning from superhydrophobic plants: the use of hydrophilic areas on superhydrophobic surfaces for droplet control part of the "Langmuir 25th year: wetting and superhydrophobicity" special issue. *Langmuir*, **25**(24), 14121–14128.

9 Barthlott, W. and Neinhuis, C. (1997) Purity of the sacred lotus, or escape from contamination in biological surfaces. *Planta*, **202**(1), 1–8.

10 Holloway, P.J. (1994) in *Air Pollution and the Leaf Cuticle* (eds K.E. Percy, J.N. Cape, R. Jagels, and C.J. Simpson), Springer, Berlin, pp. 1–13.

11 Martin, J.T. and Juniper, B.E. (1970) *The Cuticles of Plants*, Edward Arnold, London.

12 Ma, M. and Hill, R.M. (2006) Superhydrophobic surfaces. *Curr. Opin. Colloid Interface Sci.*, **11**(4), 193–202.

13 Young, T. (1805) An essay on the cohesion of fluids. *Philos. Trans. R. Soc. London*, **95**, 65–87.

14 Bhushan, B. (2012) *Biomimetics*, (ed. B. Bhushan) Springer, Berlin, Heidelberg, pp. 49–65.

15 Wenzel, R.N. (1936) Resistance of solid surfaces to wetting by water. *Ind. Eng. Chem.*, **28**(8), 988–994.

16 Wenzel, R.N. (1949) Surface roughness and contact angle. *J. Phys. Chem.*, **53**(9), 1466–1467.

17 Gürsoy, M. and Karaman, M. (2015) Effect of substrate temperature on initiated plasma enhanced chemical vapor deposition of PHEMA thin films. *Phys. Status Solidi C*, **12**(7), 1006–1010.

18 Barshilia, H.C. and Gupta, N. (2014) Superhydrophobic polytetrafluoroethylene surfaces with leaf-like micro-protrusions through Ar+O_2 plasma etching process. *Vacuum*, **99**, 42–48.

19 Jin, M., Feng, X., Xi, J., Zhai, J., Cho, K., Feng, L., and Jiang, L. (2005) Super-hydrophobic PDMS surface with ultra-low adhesive force. *Macromol. Rapid Commun.*, **26**(22), 1805–1809.

20 Ma, M., Mao, Y., Gupta, M., Gleason, K.K., and Rutledge, G.C. (2005) Super-hydrophobic fabrics produced by electrospinning and chemical vapor deposition. *Macromolecules*, **38**(23), 9742–9748.

21 Liu, Y., Chen, X., and Xin, J.H. (2006) Super-hydrophobic surfaces from a simple coating method: a bionic nanoengineering approach. *Nanotechnology*, **17**(13), 3259.

22 Grewal, H.S., Piao, S., Cho, I.J., Jhang, K.Y., and Yoon, E.S. (2016) Nanotribological and wetting performance of hierarchical patterns. *Soft Matter*, **12**(3), 859–866.

23 Sun, M., Luo, C., Xu, L., Ji, H., Ouyang, Q., Yu, D., and Chen, Y. (2005) Artificial lotus leaf by nanocasting. *Langmuir*, **21**(19), 8978–8981.

24 Cassie, A.B.D. and Baxter, S. (1944) Wettability of porous surfaces. *Trans. Faraday Soc.*, **40**, 546–551.

25 Bhushan, B. and Her, E.K. (2010) Fabrication of superhydrophobic surfaces with high and low adhesion inspired from rose petal. *Langmuir*, **26**(11), 8207–8217.

26 Bico, J., Thiele, U., and Quéré, D. (2002) Wetting of textured surfaces. *Colloids Surf., A*, **206**(1), 41–46.

27 Feng, L., Zhang, Y., Xi, J., Zhu, Y., Wang, N., Xia, F., and Jiang, L. (2008) Petal effect: a superhydrophobic state with high adhesive force. *Langmuir*, **24**(8), 4114–4119.

28 Karaman, M., Çabuk, N., Özyurt, D., and Köysüren, Ö. (2012) Self-supporting superhydrophobic thin polymer sheets that mimic the nature's petal effect. *Appl. Surf. Sci.*, **259**, 542–546.

29 Guangming, G., Juntao, W., Yong, Z., Jingang, L., Xu, J., and Lei, J. (2014) A novel fluorinated polyimide surface with petal effect produced by electrospinning. *Soft Matter*, **10**(4), 549–552.

30 Liu, Y., Li, S., Zhang, J., Wang, Y., Han, Z., and Ren, L. (2014) Fabrication of biomimetic superhydrophobic surface with controlled adhesion by electrodeposition. *Chem. Eng. J.*, **248**, 440–447.

31 Xie, L., Tang, Z., Jiang, L., Breedveld, V., and Hess, D.W. (2015) Creation of superhydrophobic wood surfaces by plasma etching and thin-film deposition. *Surf. Coat. Technol.*, **281**, 125–132.

32 Xia, D., Johnson, L.M., and López, G.P. (2012) Anisotropic wetting surfaces with one-dimensional and directional structures: fabrication approaches, wetting properties and potential applications. *Adv. Mater.*, **24**(10), 1287–1302.

33 Wang, S., Liu, K., Yao, X., and Jiang, L. (2015) Bioinspired surfaces with superwettability: new insight on theory, design, and applications. *Chem. Rev.*, **115**(16), 8230–8293.

34 Feng, L., Li, S., Li, Y., Li, H., Zhang, L., Zhai, J., Song, Y., Liu, B., Jiang, L., and Zhu, D. (2002) Super-hydrophobic surfaces: from natural to artificial. *Adv. Mater.*, **14**(24), 1857–1860.

35 Yao, J., Wang, J., Yu, Y., Yang, H., and Xu, Y. (2012) Biomimetic fabrication and characterization of an artificial rice leaf surface with anisotropic wetting. *Chin. Sci. Bull.*, **57**(20), 2631–2634.

36 Yang, X., Song, J., Xu, W., Liu, X., Lu, Y., and Wang, Y. (2013) Anisotropic sliding of multiple-level biomimetic rice-leaf surfaces on aluminium substrates. *IET Micro Nano Lett.*, **8**(11), 801–804.

37 Zhu, D., Li, X., Zhang, G., Zhang, X., Zhang, X., Wang, T., and Yang, B. (2010) Mimicking the rice leaf from ordered binary structures to anisotropic wettability. *Langmuir*, **26**(17), 14276–14283.

38 Wu, S.Z., Wu, D., Yao, J., Chen, Q.D., Wang, J.N., Niu, L.G., Fang, H.H., and Sun, H.B. (2010) One-step preparation of regular micropearl arrays for two-direction controllable anisotropic wetting. *Langmuir*, **26**(14), 12012–12016.

39 Clasen, T., Pruss-Ustun, A., Mathers, C.D., Cumming, O., Cairncross, S., and Colford, J.M. (2014) Estimating the impact of unsafe water, sanitation and hygiene on the global burden of disease: evolving and alternative methods. *Trop. Med. Int. Health*, **19**(8), 884–893.

40 World Health Organization (2014) UN-water global analysis and assessment of sanitation and drinking-water, in *Investing in Water and Sanitation: Increasing Access, Reducing Inequalities*, World Health Organization, Geneva.

41 WHO/UNICEF Joint Water Supply, Sanitation Monitoring Programme, & World Health Organization (2014) *Progress on drinking water and sanitation: 2014 Update*, World Health Organization.

42 Parker, A.R. and Lawrence, C.R. (2001) Water capture by a desert beetle. *Nature*, **414**(6859), 33–34.

43 Zhai, L., Berg, M.C., Cebeci, F.C., Kim, Y., Milwid, J.M., Rubner, M.F., and Cohen, R.E. (2006) Patterned superhydrophobic surfaces: toward a synthetic mimic of the Namib Desert beetle. *Nano Lett.*, **6**(6), 1213–1217.

44 Garrod, R.P., Harris, L.G., Schofield, W.C.E., McGettrick, J., Ward, L.J., Teare, D.O.H., and Badyal, J.P.S. (2007) Mimicking a stenocara beetle's back for microcondensation using plasmachemical patterned superhydrophobic-superhydrophilic surfaces. *Langmuir*, **23**(2), 689–693.

45 Dorrer, C. and Rühe, J. (2008) Mimicking the stenocara beetle dewetting of drops from a patterned superhydrophobic surface. *Langmuir*, **24**(12), 6154–6158.

46 Ju, J., Bai, H., Zheng, Y., Zhao, T., Fang, R., and Jiang, L. (2012) A multi-structural and multi-functional integrated fog collection system in cactus. *Nat. Commun.*, **3**, 1247.

47 Lorenceau, É. and Quéré, D. (2004) Drops on a conical wire. *J. Fluid Mech.*, **510**, 29–45.

48 Bai, H., Tian, X., Zheng, Y., Ju, J., Zhao, Y., and Jiang, L. (2010) Direction controlled driving of tiny water drops on bioinspired artificial spider silks. *Adv. Mater.*, **22**(48), 5521–5525.

49 Cao, M., Ju, J., Li, K., Dou, S., Liu, K., and Jiang, L. (2014) Facile and large-scale fabrication of a cactus-inspired continuous fog collector. *Adv. Funct. Mater.*, **24**(21), 3235–3240.

50 Andrews, H.G., Eccles, E.A., Schofield, W.C.E., and Badyal, J.P.S. (2011) Three-dimensional hierarchical structures for fog harvesting. *Langmuir*, **27**(7), 3798–3802.

51 Phillips, M.B. and Jiang, P. (2013) in *Engineered Biomimicry* (eds A. Lakhtakia and R.J. Martin-Palma), Elsevier, pp. 305–331.

52 Parker, A.R. and Townley, H.E. (2007) Biomimetics of photonic nanostructures. *Nat. Nanotechnol.*, **2**(6), 347–353.

53 Southwell, W.H. (1991) Pyramid-array surface-relief structures producing antireflection index matching on optical surfaces. *J. Opt. Soc. Am. A*, **8**(3), 549–553.

54 Kwon, Y.W., Park, J., Kim, T., Kang, S.H., Kim, H., Shin, J., Jeon, S., and Hong, S.W. (2016) Flexible near-field nanopatterning with ultrathin, conformal phase masks on non-planar substrates for biomimetic hierarchical photonic structures. *ACS Nano*, **10**(4), 4609–4617.

55 Raut, H.K., Dinachali, S.S., Loke, Y.C., Ganesan, R., Ansah-Antwi, K.K., Góra, A., Khoo, E.H., Ganesh, V.A., Saifullah, M.S., and Ramakrishna, S. (2015) Multiscale ommatidial arrays with broadband and omnidirectional antireflection and antifogging properties by sacrificial layer mediated nanoimprinting. *ACS Nano*, **9**(2), 1305–1314.

56 Oh, S.S., Choi, C.G., and Kim, Y.S. (2010) Fabrication of micro-lens arrays with moth-eye antireflective nanostructures using thermal imprinting process. *Microelectron. Eng.*, **87**(11), 2328–2331.

57 Li, T., Lou, S., Ding, J., and Fan, T. (2014) Antireflective amorphous carbon nanocone arrays inspired from compound eyes. *Bioinspir. Biomim. Nan.*, **3**(1), 29–37.

58 Xu, H., Lu, N., Shi, G., Qi, D., Yang, B., Li, H., Xu, W., and Chi, L. (2011) Biomimetic antireflective hierarchical arrays. *Langmuir*, **27**(8), 4963–4967.

59 Zhu, C. and Gu, Z.Z. (2012) in *Bioinspiration and Biomimicry in Chemistry: Reverse-Engineering Nature* (ed. G. Swiegers), John Wiley & Sons, Inc., pp. 293–322.

60 Young, A.M. (1971) Wing coloration and reflectance in Morpho butterflies as related to reproductive behavior and escape from avian predators. *Oecologia*, **7**(3), 209–222.

61 Dushkina, N. and Lakhtakia, A. (2013) in *Engineered Biomimicry*, (*eds* A. Lakhtakia *and* R.J. Martin-Palma), Elsevier, pp. 267-303.

62 Sun, J., Bhushan, B., and Tong, J. (2013) Structural coloration in nature. *RSC Adv.*, **3**(35), 14862–14889.

63 Parker, A.R. (2000) 515 million years of structural colour. *J. Opt. A: Pure Appl. Opt.*, **2**(6), R15–R28.

64 Saito, A. (2005) in *Structural Colors in Biological Systems* (eds S. Kinoshita and S. Yoshioka), Osaka University Press, Osaka, p. 287.

65 Kinoshita, S. (ed.) (2013) *Bionanophotonics: an Introductory Textbook*, CRC Press.

66 Jiang, T., Peng, Z., Wu, W., Shi, T., and Liao, G. (2014) Gas sensing using hierarchical micro/nanostructures of Morpho butterfly scales. *Sens. Actuators, A*, **213**, 63−69.

67 Anderson, T.F. and Richards, A.G. Jr., (1942) An electron microscope study of some structural colors of insects. *J. Appl. Phys.*, **13**(12), 748−758.

68 Watanabe, K., Hoshino, T., Kanda, K., Haruyama, Y., and Matsui, S. (2005) Brilliant blue observation from a morpho- butterfly-scale quasi-structure. *Jpn. J. Appl. Phys.*, **44**, L48−L50.

69 Saito, A., Yoshioka, S., and Kinoshita, S. (2004) Reproduction of the *Morpho* butterfly's blue: arbitration of contradicting factors, in *Proceedings of SPIE (Optical Systems Degradation, Contamination, and Stray Light: Effects, Measurements, and Control)* (eds P.T.C. Chen, J.C. Fleming, and M.G. Dittman), SPIE, Bellingham, WA, pp. 188−194.

70 Cong, H. and Cao, W. (2004) Thin film interference of colloidal thin films. *Langmuir*, **20**(19), 8049−8053.

71 Eadie, L. and Ghosh, T.K. (2011) Biomimicry in textiles: past, present and potential. An overview. *J. R. Soc. Interface*, **8**(59), 761−775.

72 Bhushan, B. (ed.) (2012) *Encyclopedia of Nanotechnology*, Springer, Dordrecht, Netherlands.

73 Bhushan, B. (2012) Bioinspired structured surfaces. *Langmuir*, **28**(3), 1698−1714.

74 Chen, P.Y., McKittrick, J., and Meyers, M.A. (2012) Biological materials: functional adaptations and bioinspired designs. *Prog. Mater Sci.*, **57**(8), 1492−1704.

75 Bechert, D.W., Bruse, M., and Hage, W. (2000) Experiments with three-dimensional riblets as an idealized model of shark skin. *Exp. Fluids*, **28**(5), 403−412.

76 Liu, K. and Jiang, L. (2012) Bio-inspired self-cleaning surfaces. *Annu. Rev. Mater. Res.*, **42**, 231−263.

77 Lee, M. (2014) in *Remarkable Natural Material Surfaces and Their Engineering Potential* (ed. M. Lee), Springer International Publishing, pp. 15−27.

78 Bhushan, B. (2009) Biomimetics: lessons from nature–an overview. *Philos. Trans. R. Soc. London, Ser. A*, **367**(1893), 1445−1486.

79 Biomimicry Institute www.biomimicryinstitute.org (accessed 3 January 2016).

80 Carman, M.L., Estes, T.G., Feinberg, A.W., Schumacher, J.F., Wilkerson, W., Wilson, L.H., Callow, M.E., Callow, J.A., and Brennan, A.B. (2006) Engineered antifouling microtopo- graphies – correlating wettability with cell attachment. *Biofouling*, **22**(1), 11−21.

81 Wen, L., Weaver, J.C., and Lauder, G.V. (2014) Biomimetic shark skin: design, fabrication and hydrodynamic function. *J. Exp. Biol.*, **217**(10), 1656−1666.

82 Han, X., Zhang, D., Li, X., and Li, Y. (2008) Bio-replicated forming of the biomimetic drag-reducing surfaces in large area based on shark skin. *Chin. Sci. Bull.*, **53**(10), 1587−1592.

83 Chen, H., Rao, F., Shang, X., Zhang, D., and Hagiwara, I. (2013) Biomimetic drag reduction study on herringbone riblets of bird feather. *J. Bionic Eng.*, **10** (3), 341–349.

84 Smith, M.A., Jones, N.M.M. II, Page, S.L., and Dirda, M.P. (1984) Pressure-sensitive tape and techniques for its removal from paper. *J. Am. Inst. Conserv.*, **23**(2), 101–113, Article 3.

85 Qu, L., Li, Y., and Dai, L. (2012) Bioinspired surfaces I: gecko-foot mimetic adhesion, in *Bioinspiration and Biomimicry in Chemistry: Reverse-Engineering Nature* (ed. G. Swiegers), John Wiley and Sons, pp. 251–291.

86 Barnes, W.J.P. (2012) in *Encyclopedia of Nanotechnology* (ed. B. Bhushan), Springer, Dordrecht, Netherlands, pp. 70–83.

87 Eisner, T. and Aneshansley, D.J. (2000) Defense by foot adhesion in a beetle (*Hemisphaerota cyanea*). *Proc. Natl. Acad. Sci. U.S.A.*, **97**(12), 6568–6573.

88 Autumn, K. and Gravish, N. (2008) Gecko adhesion: evolutionary nanotechnology. *Philos. Trans. R. Soc. London, Ser. A*, **366**(1870), 1575–1590.

89 Autumn, K. (2006) How gecko toes stick the powerful, fantastic adhesive used by geckos is made of nanoscale hairs that engage tiny forces, inspiring envy among human imitators. *Am. Sci.*, **94**(2), 124–132.

90 Lee, M. (2014) in *Remarkable Natural Material Surfaces and Their Engineering Potential* (ed. M. Lee), Springer International Publishing, pp. 115–126.

91 Varenberg, M., Pugno, N.M., and Gorb, S.N. (2010) Spatulate structures in biological fibrillar adhesion. *Soft Matter*, **6**(14), 3269–3272.

92 Qu, L. and Dai, L. (2007) Gecko-foot-mimetic aligned single-walled carbon nanotube dry adhesives with unique electrical and thermal properties. *Adv. Mater.*, **19**(22), 3844–3849.

93 Cho, W.K. and Choi, I.S. (2008) Fabrication of hairy polymeric films inspired by geckos: wetting and high adhesion properties. *Adv. Funct. Mater.*, **18**(7), 1089–1096.

94 Davies, J., Haq, S., Hawke, T., and Sargent, J.P. (2009) A practical approach to the development of a synthetic Gecko tape. *Int. J. Adhes. Adhes.*, **29**(4), 380–390.

95 Kustandi, T.S., Samper, V.D., Yi, D.K., Ng, W.S., Neuzil, P., and Sun, W. (2007) Self-assembled nanoparticles based fabrication of Gecko foot-hair-inspired polymer nanofibers. *Adv. Funct. Mater.*, **17**(13), 2211–2218.

96 Geim, A.K., Dubonos, S.V., Grigorieva, I.V., Novoselov, K.S., Zhukov, A.A., and Shapoval, S.Y. (2003) Microfabricated adhesive mimicking gecko foot-hair. *Nat. Mater.*, **2**(7), 461–463.

97 Kim, T.I., Jeong, H.E., Suh, K.Y., and Lee, H.H. (2009) Stooped nanohairs: geometry-controllable, unidirectional, reversible, and robust gecko-like dry adhesive. *Adv. Mater.*, **21**(22), 2276–2281.